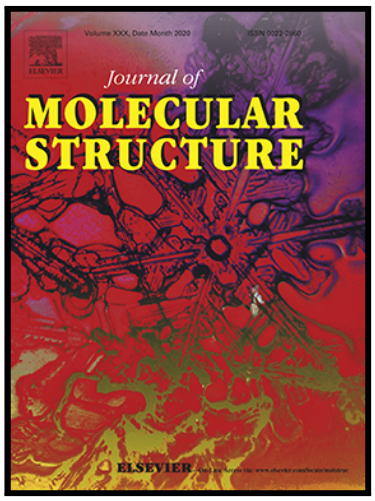

Diverse structural assemblies of a series of ninhydrin derivatives: Quantitative analyses from experimental and theoretical studies

Yeshwinder Saini , Sheena Mahajan , Kamal K. Kapoor , Geeta Hundal , Saikat Kumar Seth

PII: S0022-2860(20)31245-X
DOI: https://doi.org/10.1016/j.molstruc.2020.128920
Reference: MOLSTR 128920

To appear in: *Journal of Molecular Structure*

Received date: 18 May 2020
Revised date: 15 July 2020
Accepted date: 15 July 2020

Please cite this article as: Yeshwinder Saini , Sheena Mahajan , Kamal K. Kapoor , Geeta Hundal , Saikat Kumar Seth , Diverse structural assemblies of a series of ninhydrin derivatives: Quantitative analyses from experimental and theoretical studies, *Journal of Molecular Structure* (2020), doi: https://doi.org/10.1016/j.molstruc.2020.128920

Highlights

- Newer ninhydrin derivatives have been studied.
- Supramolecular self-assembly of the X-ray structure were explored in detail.
- Hirshfeld surface and Energy framework analysis were performed.
- DFT calculation were performed to explore the energetic features.
- Bader's theory of "atoms-in-molecules" (AIM) have been performed.

Diverse structural assemblies of a series of ninhydrin derivatives: Quantitative analyses from experimental and theoretical studies

Yeshwinder Saini,[a] Sheena Mahajan,[a] Kamal K. Kapoor,[a,*] Geeta Hundal,[b] Saikat Kumar Seth,[c,*]

[a]*Department of Chemistry, University of Jammu, Jammu-180 006, India*

[b]*Department of Chemistry, Guru Nanak Dev University, Amritsar-143 005, India*

[c] *Department of Physics, Jadavpur University, Kolkata 700032, India*

Corresponding author(s) E-mail: k2kapoor@yahoo.com (K.K. Kapoor) and saikatk.seth@jadavpuruniversity.in (S.K.S)

Abstract: Three ninhydrin derivatives (**2**–**4**) have been synthesized where the reaction of ninhydrin with Meldrum's acid yielded [3.3.3] propellanoid (**2**) and ethyl 2,2-bis (1,3-dioxo-2,3-dihydro-1*H*-inden-2-yl)acetate (**3**) while with malononitrile yielded a spiroindenopyran (**4**). The products being crystalline in nature and are characterized by single crystal X-ray diffraction in addition to other spectroscopic studies. X-ray crystallography reveals that solid-state structure of the title compounds exhibits C–H···π, π–π and lone-pair(l.p)···π interactions in building supramolecular assemblies. Indeed, compound (**2**) was stabilized through extended supramolecular C–H···π/π–π/π···H–C network whereas compounds (**3**) and (**4**) are stabilized through lone-pair (l.p)···π and π–π interaction respectively. The diverse intermolecular interactions *via* Hirshfeld surface analysis enables quantitative contributions to the crystal packing that exposes the similarities and differences in the interactions experienced by each compound. The distinctive energy frameworks have been calculated for individual molecules and the interaction energies suggest that the contacts are largely dispersive in nature. The binding energies associated with the non-covalent interactions observed in the crystal structures have been calculated using theoretical DFT calculations. Finally, the interplay between the interactions have been characterized by Bader's theory of "atoms-in-molecules" (AIM).

***Keywords*:** Ninhydrin derivatives; Supramolecular self-assembly; Hirshfeld surface; Energy Framework; DFT calculation; 'atoms-in-molecules' (AIM).

1. Introduction

Propellanes constitute a unique class of polycyclic hydrocarbons possessing two more or less inverted tetrahedral carbon atoms common to three bridging rings. Among these, smaller entities have significantly weakened central single bond between the two bridgeheads leading to unusual reactivity of these structurally fascinating propeller-like molecules. Various biologically active natural products such as modhephene (**1A**)[1], hasubanan alkaloids(**1B**)[2], merrilactone A (**1C**)[3] and periglaucine A (**1D**)[4] contain propellanoid motif (**Fig. 1**) and so are the molecules with spiro framework having applications as organic light-emitting diode (OLED)[5], as fluorescent probe [fluorescamine(**1E**)] (**Fig. 1**) for peptides, proteins and primary amines [6], anti-bacterial[7], anti-influenza[8] and inhibitory agents against enzymatic activity of *t*RNA synthetase[9]. Synthesis of propellanes and spiro compounds poses an extraordinarily challenge for the researchers [10]. As a part of research in developing newer methodologies for the unprecedented synthesis of newer oxygen containing heterocyclic compounds[11], reaction of ninhydrin with active methylenes has been utilized. To further explore the potential of this chemistry, reaction of ninhydrin with Meldrum's acid and malononitrile was conceived to access propellanes and spiro heterocycles.

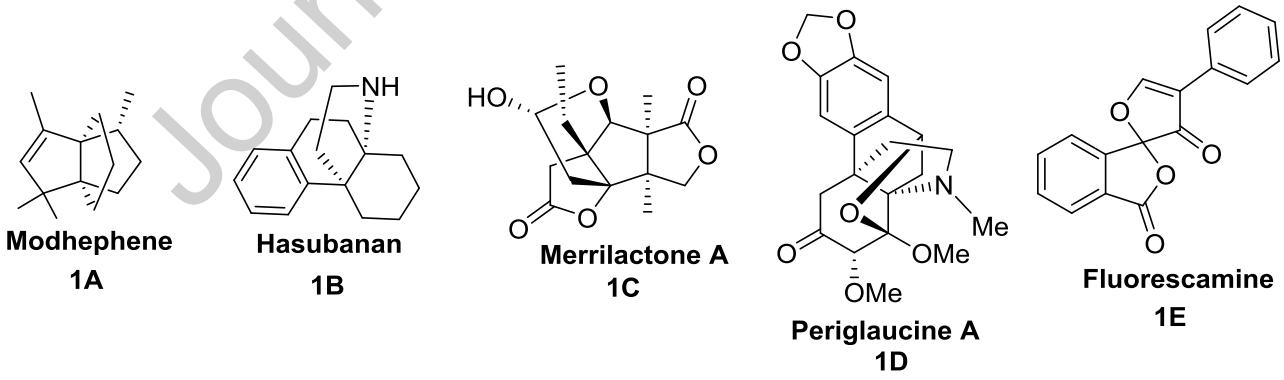

Fig. 1 Some significant compounds 1(A-E) containing propellane and spiro moieties.

The detailed understanding of weak interactions are essential to develop new application in supramolecular chemistry across a variety of fields [12-15]. The properties of a crystalline

solid intensely depend on how the molecules are organized and the control over this organization directs the functional properties of the material. Crystals are assembled in spontaneous process and the recognition between set of molecules is the consequence of the mutual interaction through various forces. Hydrogen bonding is the non-covalent interaction that usually dominates the crystal packing due to directionality and strength [16-18]. Though hydrogen bonding has been widely employed in crystal packing, other weaker forces involving aromatic rings are also important players in crystal engineering [19]. For instance, C–H···π [20], π–π [21-24], anion···π [25-28] and lone-pair(l.p)···π [29-32] are commonly used to explore solid-state networks [33]. Herein, we report the X-ray characterization of three ninhydrin compounds by exploring their supramolecular assemblies involving weak forces. The solid-state structures are described in detail; the binding energies of the networks have been calculated using theoretical DFT calculations. Finally, the non-covalent interactions have been characterized by using Bader's theory of "Atoms in molecules" (AIM).

2. Experimental sections

2.1. Experimental

2.1.1. General procedures

All the experiments were performed in an oven dried glass apparatus. All the commercially available reagents were purchased from *Aldrich* and were used without further purification. Ultrasonication was performed on 2510 Branson Ultrasonicator. The progress of reaction was monitored by thin layer chromatography (TLC) using silica gel pre-coated aluminium sheets (60 F254, Merck). Visualization of spots was effected by exposure to ultraviolet light (UV) at 365 nm and 254 nm, iodine vapours and 2% 2,4-dinitrophenylhydrazine in methanol containing few drops of H_2SO_4 and draggendroff reagent.

2.1.2. Syntheses

2.1.2.1. Procedure for the synthesis of (2) and (3)

A mixture of ninhydrin (0.89g, 5 mmol) and Meldrum's acid (2.16g, 15 mmol) was ultrasonicated in ethanol (30 ml). After three hours ethanol was removed and the residue was subjected to column chromatography to yield three products *i.e.* malonic acid (0.21g, 40%), (**2**) (0.187g, 13%) and (**3**) (0.282g, 30%) respectively. (**2**) and (**3**) were further purified by recrystallization with ethanol.

2.1.2.2. Procedure for the synthesis of (4A) and (4)

0.89g (5 mmol) of ninhydrin and 0.99g (15 mmol) of malononitrile were added to 70 ml of distilled water and the mixture was stirred and boiled for 20 minutes. The solid separated was filtered, dried and recrystallized from acetonotrile to yield two types of crystalline products, interestingly distinguishable by color (orange and yellow). The products were isolated manually, thereby, avoiding the use of column chromatography. The products could also be isolated by column chromatography using gradient mixture of ethyl acetate and petroleum ether.

2.2. Characterization

2.2.1. Measurements

Melting points (°C) were measured in open glass capillaries using Perfit melting point apparatus and are uncorrected. IR spectra (ν, cm^{-1}) were recorded on Perkin-Elmer FTIR spectrophotometer using KBr discs. ^{1}H and ^{13}C NMR were recorded on Bruker AC-400 spectrometer operating at 400 MHz for ^{1}H and 100 MHz for ^{13}C with tetramethylsilane (TMS) as an internal standard. All the ^{13}C NMR spectra are proton decoupled. The chemical shifts are expressed in δ (ppm) downfield from TMS. *J* values are given in Hertz (Hz). The abbreviations s, d, t, q and m in ^{1}H NMR spectra refer to singlet, doublet, triplet, quartet and multiplet respectively. ESI-MS were recorded on Micro Mass VG-7070 H mass spectrometer. Commercial grade solvents were dried as per established procedure before use [34]. Elemental analysis was performed on Leco CHNS 932 analyzer. Solvents were removed using Heidolph rotary vapour.

2.2.2. Spectroscopic measurements

2-Ethoxy-2-methyl-2H-3a,8b-(epoxyethano)indeno[1,2-b]furan-4,10(3H)-dione(2)

White crystalline solid (0.187g, 13% yield); Mp 295°C; **^{1}H NMR** (400 MHz, CD_3OD) δ 7.95-7.77 (m, 3H), 7.68- 7.60 (m, 1H), 4.17-4.07 (q, *J* = 8 Hz, 2H), 3.46-3.40 (d, *J* = 16 Hz, 1H), 3.17-3.08 (d, *J* = 20 Hz, 1H), 2.82-2.75 (d, *J* = 12 Hz, 1H), 2.49-2.42 (d, *J* = 12 Hz, 1H), 1.52-1.48 (s, 3H), 1.34-1.23 (m, 3H); **^{13}C NMR** (100 MHz, CD_3OD) δ 196.04, 173.62, 152.72, 136.83, 130.30, 125.09, 124.78, 110.61, 94.64, 89.12, 56.27, 48.26, 42.33, 21.30, 13.68. **IR**(KBr)ν_{max}/cm^{-1}: 3400.40, 2923.71, 1795.99, 1730.98, 1046.66,

1019.79; *Anal.* calcd. for $C_{16}H_{16}O_5$: C, 66.66; H, 5.59; found C, 66.42; H, 5.66; **ESI-MS***(m/z)*: $[M+H]^+$ = 289.

Ethyl 2,2-bis(1,3-dioxo-2,3-dihydro-1H-inden-2-yl)acetate (3)

White crystalline solid (0.282g, 30% yield); Mp 198-200 °C; **^{1}H NMR** (400 MHz, $CDCl_3$) δ 8.06-7.98 (d, *J* = 7.4 Hz, 2H), 7.94-7.74 (m, 6H), 4.23-4.19 (t, 1H, *J* = 4 Hz), 4.18-4.10 (q, 2H, *J* = 8 Hz), 3.72-3.65 (d, 2H, *J* = 4 Hz) 1.16-1.08 (t, 3H, *J* = 8 Hz);**^{13}C NMR** (100 MHz, $CDCl_3$) δ 198.24, 196.62, 170.68, 142.48, 141.47, 135.75, 135.27, 123.36, 123.24, 62.01, 51.35, 40.43, 13.72.**IR**(KBr)ν_{max}/cm^{-1}: 3443.45, 1748.25, 1711.22; *Anal.* calcd. for $C_{22}H_{16}O_6$:C, 70.21; H, 4.29; found C, 70.35; H, 4.19; **ESI-MS***(m/z)* : $[M+H]^+$ = 377, $[M+Na]^+$ = 399, $[M\text{-}COOEt]^+$ = 303.

2-(1,3-Dioxo-1H-inden-2(3H)-ylidene)malononitrile (4A). Yellow colored crystalline solid (0.74g, 71% yield): mp 267-268°C (lit. 267-268°C)[10(d)]; **^{1}H NMR** (400 MHz, DMSO-d_6) δ 8.07-7.98 (m, 4H); **^{13}C NMR** (100 MHz, DMSO-d_6) δ 182.47, 152.51, 141.75, 137.91, 128.34, 124.55, 110.42, 88.80; **IR**(KBr)ν_{max}/cm^{-1}: 1705.05, 1618.90 cm^{-1} ; *Anal.* calcd. for $C_{12}H_4N_2O_2$:C, 69.24; H, 1.94; N, 13.46; O, 15.37; found C, 69.35; H, 1.85; N, 13.52; O, 15.21; **ESI-MS** (m/z) : $[M+H]^+$, 209.

2'-Amino-1,3,5'-trioxo-1,3-dihydro-5'H-spiro[indene-2,4'-indeno[1,2-b]pyran]-3'-carbonitrile (4). Orange colored crystalline solid (0.16g, 18% yield): mp 259°C (lit. 255-260°C) [13]; **^{1}H NMR** (400 MHz, DMSO-d_6) δ 8.14 (d, *J* = 6.6 Hz, 2H), 8.02 – 7.87 (m, 4H), 7.73 (d, *J* = 8.6 Hz, 2H), 6.95 (d, *J* = 8.6 Hz, 12H), 3.79 (s, 2H); **^{13}C NMR** (100 MHz, DMSO-d_6) δ 194.80, 189.97, 177.03, 150.72, 147.46, 138.22, 134.06, 132.37, 131.57, 131.11, 130.81, 130.48, 129.26, 127.88, 126.79, 126.07, 125.94, 125.04, 124.65, 75.36, 57.03; **IR**(KBr)ν_{max}/cm^{-1}: 3435.90, 1635.83; *Anal.*calcd. for $C_{21}H_{10}N_2O_4$:C, 71.19; H, 2.84; N, 7.91; O, 18.06; found C, 70.35; H, 2.38; N, 7.46; O, 17.95; **ESI-MS** (m/z) : $[M+H]^+$, 355.

2.2.3. X-ray crystal structure determination

Single crystal X-ray data of compounds (**2**–**4**) were collected on a Bruker Kappa Apex-II diffractometer at room temperature with Mo-Kα radiation (λ = 0.71073 Å). Data reduction was carried out using the program Bruker SAINT [35] and an empirical absorption correction was applied based on the multi-scan method [36]. The structures of the title compounds were solved

by the direct method and refined by the full-matrix least-square technique on F^2 using the programs (SHELXS-14) [37] and (SHELXL-18) [38] respectively. All the non-H atoms were treated anisotropically and all H atoms were attached geometrically. The summary of crystal data and relevant structure refinement parameters of the title compounds are given in Table 1. CCDC 1900911, 1900913 and 1900912 contain the supplementary crystallographic data of compounds (**2**–**4**) respectively.

Table 1. Crystal data and structure refinement parameters for the title compounds.

Structure	**(2)**	**(3)**	**(4)**
Empirical formula	$C_{16}H_{16}O_5$	$C_{22}H_{16}O_6$	$C_{21}H_{10}N_2O_4$
Formula Weight	288.29	376.36	354.31
Temperature (K)	295(2)	296(2)	296(2)
Wavelength (Å)	0.71069	0.71073	0.71073
Crystal system	Monoclinic	Monoclinic	Monoclinic
space group	$P2_1/c$	$P2_1/n$	$P2_1/c$
a, b, c (Å)	11.997(3), 7.549(4), 16.365(5)	13.561(5), 9.021(4), 14.700(7)	10.2703(7), 16.8077(9), 9.5361(6)
α, β, γ (°)	90, 109.597(5), 90	90, 94.872(15), 90	90, 104.813(2), 90
Volume (Å^3)	1396.3(9)	1791.8(13)	1591.41(17)
Z / Density (calc.) (Mg/m^3)	4 / 1.371	4 / 1.395	4 / 1.479
Absorption coefficient (mm^{-1})	0.102	0.102	0.105
F(000)	608	784	728
Crystal size (mm^3)	0.15 × 0.12 × 0.08	0.13 × 0.11 × 0.06	0.14 × 0.08 × 0.06
Limiting indices	-14<=h<=14, -8<=k<=7, -18<=l<=19	-16<=h<=16, -10<=k<=10, -17<=l<=17	-13<=h<=13, -15<=k<=22, -10<=l<=12
Reflections collected / unique	8890 / 2488	20077 / 3250	14597 / 3753
Completeness to θ (%)	98.6	98.9	99.8
Absorption correction	Semi-empirical from equivalents	Semi-empirical from equivalents	Semi-empirical from equivalents
Max. and min. transmission	0.998 and 0.978	0.998 and 0.979	0.999 and 0.976
Refinement method	Full-matrix least-squares on F^2	Full-matrix least-squares on F^2	Full-matrix least-squares on F^2
Data / parameters	2488 / 190	3250 / 254	3753 / 0 / 250
Goodness-of - fit on F^2	0.909	0.968	1.040
Final R indices [I > 2σ(I)]	R_1 = 0.0378, wR_2 = 0.0874	R_1 = 0.0702, wR_2 = 0.1856	R_1 = 0.0427, wR_2 = 0.1032
R indices (all data)	R_1 = 0.0641, wR_2 = 0.1053	R_1 = 0.1650, wR_2 = 0.2906	R_1 = 0.0593, wR_2 = 0.1138
Largest diff. peak and hole (e.Å^{-3})	0.148 and -0.190	0.485 and -0.431	0.238 and -0.245

$R_1 = \sum||F_o|-|F_c||/\sum|F_o|$, $wR_2 = [\sum\{(F_o^2-F_c^2)^2\}/\sum\{w(F_o^2)^2\}]^{1/2}$, $w = 1/\{\sigma^2(F_o^2) + (aP)^2 + bP\}$, where a = 0.0441 and b = 0.9039 for (**2**), a = 0.1499 and b = 0.0000 for (**3**) and a = 0.0556 and b = 0.3000 for (**4**). $P = (F_o^2 + 2F_c^2)/3$ for all structures.

2.2.4. Hirshfeld surface analysis

Molecular Hirshfeld surface [39-42] is generated based on the electron distribution of the molecule and that have been calculated as the sum of spherical atom electron densities [43-44]. Hirshfeld surface is unique for a given crystal structure and a set of spherical atomic electron densities [45]. The normalized contact distance (d_{norm}) is based on d_e, d_i and the *vdW* radii of the atom. The distance d_e is defined as the distance from the point to the nearest nucleus external to

the surface, and d_i is the distance to the nearest nucleus internal to the surface. The 2D fingerprint plot (based on d_e and d_i) provides summary of intermolecular contacts in the crystal [45-47]. To explore the intermolecular interaction topology, we have performed the "energy framework analysis" using *Crystal Explorer* program [48]. The energy framework was constructed based on the crystal symmetry, in which we have used B3LYP/6-31G(d,p) molecular wave functions to estimate the interaction energies. The pair-wise interaction energy within the crystal have been calculated by summing up the electrostatic (E_{ele}), polarization (E_{pol}), dispersion (E_{dis}) and exchange-repulsion (E_{rep}) terms based on the scaling factors. The sum of the energy components (E_{tot}) for the investigating molecules are scaled following the energy model [49]. Other information like rotational symmetry operations (Symop), centroid-to-centroid distance (R) and number of pair(s) of interacting molecules (N) are also calculated for colour-coded interaction mapping. The individual energy components of the energy framework are depicted as cylinders where the radius of the cylinders are proportional to the magnitude of the interaction energy [50]. The energy components corresponding to electrostatic (E_{ele}), dispersion (E_{dis}) and total energy (E_{tot}) are represented in red, green and blue color-codes respectively.

2.2.5. Theoretical Methods

The binding energies of the title compounds included herein were performed using Gaussian 09 calculation package [51] at the B3LYP level with a large basis set 6-311++G(d,p). The visualization of the results are accomplished with GaussView 6.0. The crystallographic coordinated have been used for the theoretical analysis of the non-covalent interactions present in the solid-state structures of (**2**–**4**). The Bader's "Atoms in molecules" theory [52] has been used to investigate the interactions studied herein by means of the AIMall calculation package [53]. The topological properties of the charge density (ρ(r)) characterized by their critical points (CPs) and its Laplacian which is expressed in terms of $L(r) = -\nabla^2(\rho(r))$ were calculated using the Atom In Molecule (AIM) theory [54]. It is noted that electron density is concentrated where $\nabla^2(\rho(r)) < 0$ and it is depleted where $\nabla^2(\rho(r)) > 0$. *Gaussian09* calculation package [51] has been used for wave function analysis.

3. Results and discussion

3.1. Reaction of ninhydrin with Meldrum's acid

In continuation to our earlier work [11] that yielded unprecedented products by the reaction of ninhydrin with active methylenes on ultrasonic-irradiation, we wished to carry out the reaction of ninhydrin with Meldrum's acid. Ninhydrin was reacted with Meldrum's acid under ultrasonic-irradiation in ethanol. After 5 hours all the ninhydrin was consumed. Ethanol was removed and the residue after column chromatography gave three products (Scheme 1). The most polar product was found to be malonic acid. The remaining two products were obtained in crystalline form after recrystallization with ethanol. The less polar product was found to be ethyl 2,2-bis(1,3-dioxo-2,3-dihydro-1*H*-inden-2-yl)acetate (**3**) whereas the third polar product was found to be 2-ethoxy-2-methyl-2*H*-3a,8b-(epoxyethano)indeno[1,2-*b*]furan-4,10(3*H*)-dione (**2**) as revealed by X-ray data.

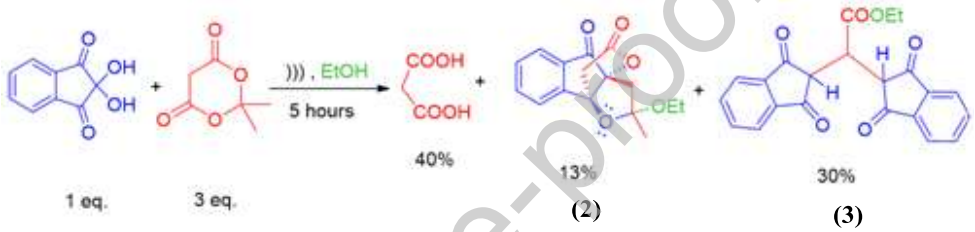

Scheme 1. Ultrasound-assisted reaction of ninhydrin with Meldrum's acid.

3.2. Reaction of ninhydrin with malononitrile

The reaction of ninhydrin with malononitrile is known to yield the single Knoevenagel product (4A) [55]. When we carried out a reaction between ninhydrin and malononitrile (1:3 ratio) using water as solvent, in addition to the Knoevenagel product (4A) (71%), we obtained an unexpected spiroindenopyran (**4**) (18%) (Scheme 2). The two products were obtained in crystalline form - the crystals of product (4A) were large block shaped and yellow in colour whereas crystals of product (**4**) were small and slightly orange in colour (Fig. S1). In our first attempt, the products were isolated manually using a spatula and forceps based on colour distinction, thus avoiding column chromatography. However, in our second attempt the products were successfully isolated by column chromatography.

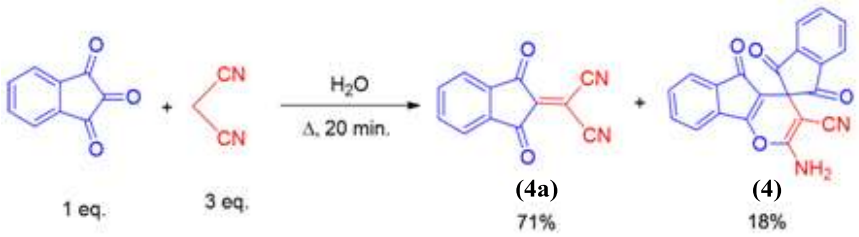

Scheme 2. Reaction between ninhydrin and malononitrile

3.3. X-ray structural description of the title compounds

3.3.1. Structural description of (2)

The molecular view of compound (**2**) is included in Fig. 2a with atom numbering scheme. The solid-state structure of (**2**) is stabilized through C–H···π and π–π interactions (Tables 2, 3). No classical hydrogen bonding interaction is observed for the title compound. The molecular packing in (**2**) is such that the π–π stacking between the aryl rings of adjacent parent and partner molecules are optimized [21-24].The aryl rings (C1–C6) of the molecule at (x, y, z) and (-x, -y, 1-z) are essentially parallel, with an interplanar spacing of 3.795(1)Å, and a ring centroid separation of 4.181Å, corresponding to a ring offset of 1.753Å. The combination of intramolecular C–H···π and intermolecular π–π stacking interactions generates C–H···π/π–π/π···H–C network in (**2**) (Fig. 2b).

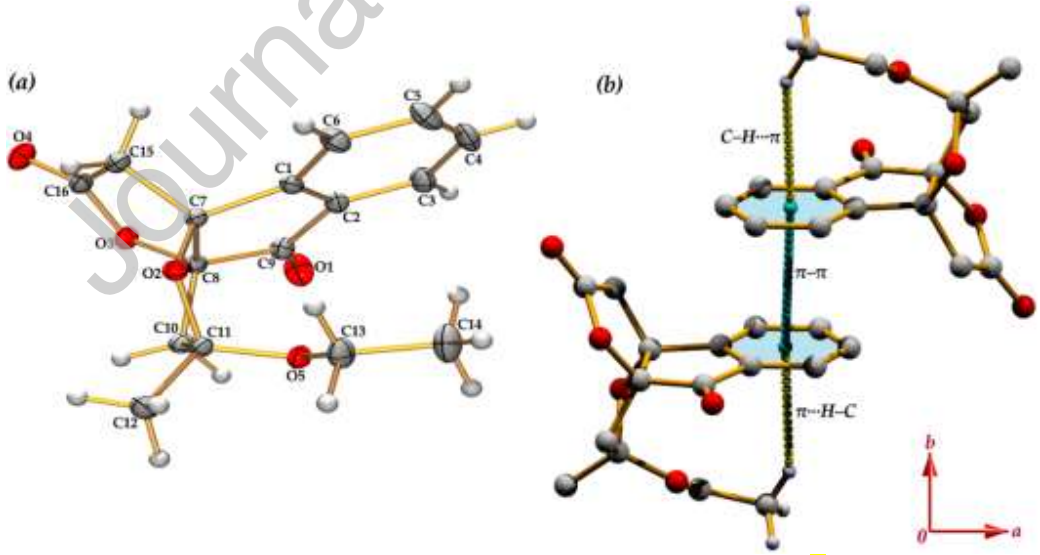

Fig. 2 (a) ORTEP view and atom numbering scheme of compound (**2**) with the displacement ellipsoid at the 30% probability level; (b) Cooperativity of weak interactions in building extended supramolecular network in (**2**).

3.3.2. Structural description of (3)

Despite the similarity between compounds (**2**) and (**3**) in terms of their overall constitutions and molecular geometries, there are some significant differences in the nature of their supramolecular aggregation. The molecular view of compound (**3**) is depicted in Fig. 3a. Compound (**3**) is stabilized through C–H···O hydrogen bonds and lone-pair(l.p)···π interactions. Due to the self-complementary nature, the carbon atom C(8) acts as donor to the carbonyl oxygen atom O(3) in the molecule at (2-x, -y, 2-z), so generating a centrosymmetric $R_2^2(12)$ dimeric ring centered at (1, 0, 1) (Fig. S2). Additional reinforcement between C15 and O4 in the molecule at (x, y, z) and (3/2-x, -1/2+y, 3/2-z) leads the molecules to generate a two-dimensional supramolecular framework in (110) plane (Fig. S2). In another substructure, the centrosymmetric dimeric rings are interconnected through C(21)–H(21)···O(6) hydrogen bonds to generate another supramolecular layered assembly in (101) plane (Fig. S3). In another substructure, the carbonyl oxygen atom is oriented towards the π-face of aryl ring (C1-C6) in the molecule at (2-x, 1-y, 2-z) with a separation distance of 3.844(5)Å, suggesting lone-pair(l.p)···π interaction [30-31]. Due to the self-complementarity, two molecules are juxtaposed through lone-pair(l.p)···π interaction by generating a centrosymmetric synthon. Moreover, another carbonyl oxygen atom O(6) is also interacting with the π-face of aryl ring at (3/2-x, 1/2+y, 3/2-z). Therefore, the additional reinforcement of lone-pair(l.p)···π interactions leads the molecules to generate a supramolecular layered assembly (Fig. 3b).

Table 2. Relevant hydrogen bonding parameters.

D–H···A	D–H	H···A	D···A	D–H···A	Symmetry
		*Compound (**2**)*			
C(14)–H(14C)···Cg(4)	0.93	2.99	3.841(4)	148	x, y, z
		*Compound (**3**)*			
C(8)–H(8)···O(3)	0.98	2.59	3.249(6)	125	x, y, z
C(8)–H(8)···O(3)	0.98	2.45	3.350(6)	152	2-x, -y, 2-z
C(15)–H(15)···O(4)	0.98	2.33	3.154(6)	141	3/2-x, -1/2+y, 3/2-z
C(21)–H(21)···O(6)	0.93	2.59	3.324(7)	137	1/2+x, 1/2-y, -1/2+z
		*Compound (**4**)*			
N(1)–H(1A)···O(1)	0.84	2.252	3.0833(17)	170	1-x, -1/2+y, 1/2-z
N(1)–H(1B)···O(4)	0.86	2.178	3.0271(18)	170	x, 1/2-y, -1/2+z
C(20)–H(20)···O(4)	0.93	2.59	3.428(2)	151	2-x, 1-y, 1-z

Cg(4) is the centroid of (C1–C6) ring.

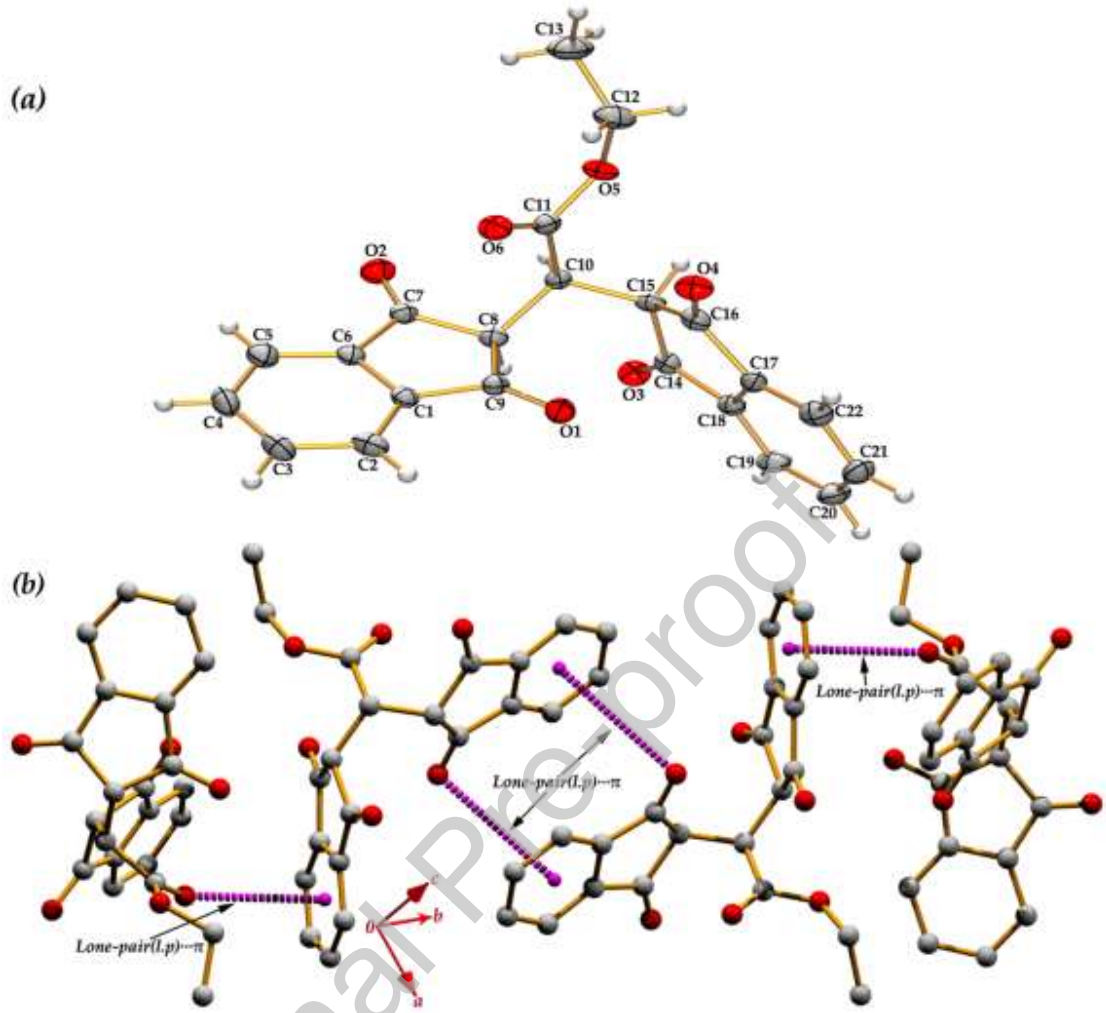

Fig. 3 (a) ORTEP view and atom numbering scheme of compound (**3**) with the displacement ellipsoid at the 30% probability level; (b) Perspective view of the supramolecular network generated through lone-pair(l.p)···π interactions in (**3**).

Table 3. Geometrical parameters (Å, °) for π-stacking interactions.

Rings i–j[a]	Rc[b]	R1v[c]	R2v[a]	α[e]	β[f]	γ[g]	Slippage
*Compound (**2**)*							
Cg(4)–Cg(4)$^{(i)}$	4.181(3)	-3.7952(10)	-3.7952(10)	0.00	24.79	24.79	1.753
*Compound (**4**)*							
Cg(5)–Cg(5)$^{(ii)}$	4.144(1)	-3.3619(6)	-3.3619(6)	0.00	35.78	35.78	2.423

[Symmetry code: (i) (-x, -y, 1-z); (ii) (x, ½-y. -1/2+z)] [a]Cg(4) and Cg(5) are the centroids of the (C1−C6) and (C14/C15/C17−C20) rings, respectively. [b]Centroid distance between ring i and ring j. [c]Vertical distance from ring centroid i to ring j. [d]Vertical distance from ring centroid j to ring i. [e]Dihedral angle between the first ring mean plane and the second ring mean plane of the partner molecule. [f]Angle between centroids of first ring and second ring mean planes. [g]Angle between the centroid of the first ring and the normal to the second ring mean plane of the partner molecule.

3.3.3. Structural description of (4)

The molecular view of compound (**4**) is shown in Fig. 4a. We have re-determined the X-ray structure [56] to quantify the non-covalent interactions in the context of crystal engineering. The title structure is stabilized through N–H···O, C–H···O hydrogen bonds, π–π interactions (Tables 2-3). The aryl ring carbon atom C(20) acts as donor to the carbonyl oxygen atom O(4) in the molecule at (2-x, 1-y, 1-z), so generating a centrosymmetric $R_2^2(10)$ dimeric ring centered at (1, ½, ½) (Fig. S4). In both side of this dimeric ring, the amine nitrogen atom N1 acts as donor to the carbonyl oxygen atom O1 at (1-x, -1/2+y, 1/2-z); thus generating a two-dimensional supramolecular framework in (110) plane (Fig. S4). In another substructure, the dimeric ring motif leads the molecules to generate an infinite chain along [001] direction (Fig. S5). Due to the self-complementarity, the parallel chains are interconnected through hydrogen bonding interaction where the amine nitrogen atom acts as donor to the carbonyl oxygen atom of the centrosymmetric ring motif. Therefore, another two-dimensional supramolecular framework is generated in the (011) plane (Fig. S5). Finally, the molecules are juxtaposed through weak π–π stacking interactions. The aryl rings (C14/C15/C17–C20) of the molecule at (x, y, z) and (x, ½-y, -1/2+z) are juxtaposed, with an interplanar spacing of 3.362(1)Å, and a ring centroid separation of 4.144Å, corresponding to a ring offset of 2.423Å (Fig. 4b).

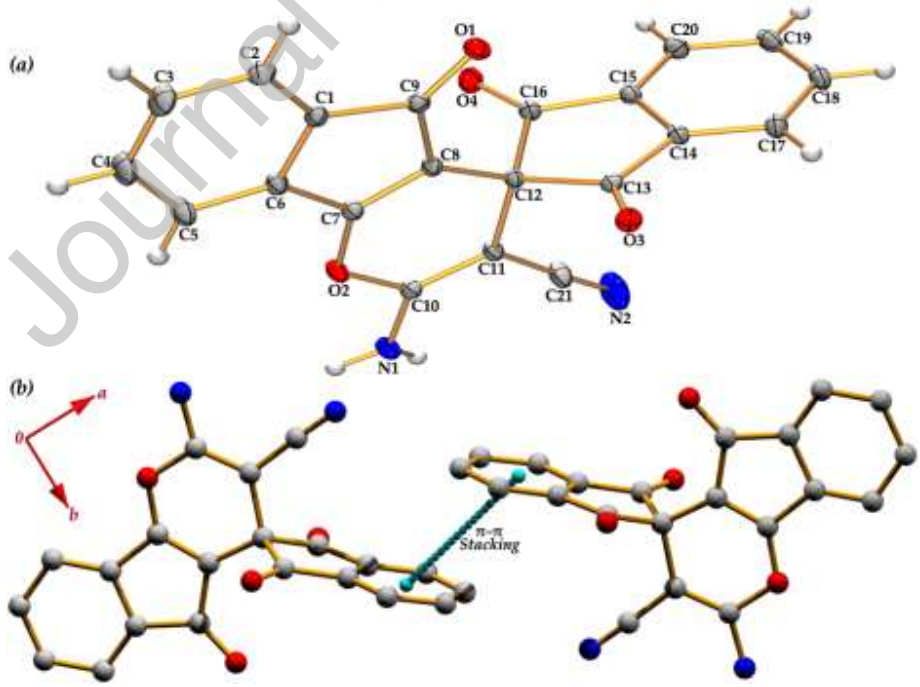

Fig. 4 (a) ORTEP view and atom numbering scheme of compound (**4**) with the displacement ellipsoid at the 30% probability level; (b) Partial view of the X-ray solid-state structure of compound (**4**).

3.4. Hirshfeld surface

The pattern of the intermolecular interactions of the solid-state structure of compounds (**2**–**4**) prompted us to explore and quantify the contribution of the non-covalent interactions. In the present study, we have evaluated the contacts that are responsible in building supramolecular assembly. The Hirshfeld surface of the title compounds are illustrated in Fig. 5 showing surfaces that have been mapped over d_{norm} [in the ranges (-0.025 to 1.504Å) in (**2**); (-0.268 to 1.221Å) in (**3**) and (-0.446 to 1.324Å) in (**4**)] and shape-index [-1.000 to 1.000Å for all compounds]. The intermolecular interactions summarized in Tables 2–3 are mostly evident by the Hirshfeld surfaces. For instance, the distinct circular depressions on the d_{norm} surface indicates the hydrogen bonding contacts whereas other small visible spots are due to short contacts. The π–π stacking has been examined and verified by the shape-index surface. The intermolecular interactions involved within the structures are also visible on the 2D fingerprint plots that can be decomposed to quantify individual contributions of intermolecular interactions (Figs. S6–S8). The distinct spikes in the full fingerprint plot of all compounds designates O···H and H···O contacts. The percentage of contacts of O···H/H···O interactions of the title compounds varies from 23.0% in (**4**) to 37.4% in (**2**). The spikes in the (d_i, d_e) region of (1.417Å, 1.121Å), (1.282Å, 0.966Å) and (1.171Å, 0.831Å) designate the O···H/H···O interaction in (**2**–**4**) respectively.

The C···H/H···C interactions appears as spoon like tips and comprises 4.3%, 18.7% and 24.2% of the total Hirshfeld surface area of (**2**–**4**) respectively (Figs. S6–S8). The spoon like tips in (**2**), sharp edged spike in (**3**) and spike in (**4**) in the (d_i, d_e) region of (1.697Å, 1.557Å), (1.763Å, 1.517Å) and (1.833Å, 1.552Å) designates C···O/O···C interactions which comprises of 1.8%, 6.5% and 5.3% to the total Hirshfeld surface area of the molecules (Figs. S6–S8). In compound (**4**), the N···H and H···N interactions are appeared in the (d_i, d_e) region of (1.432Å, 1.071Å) of the fingerprint plot (Fig. S8).

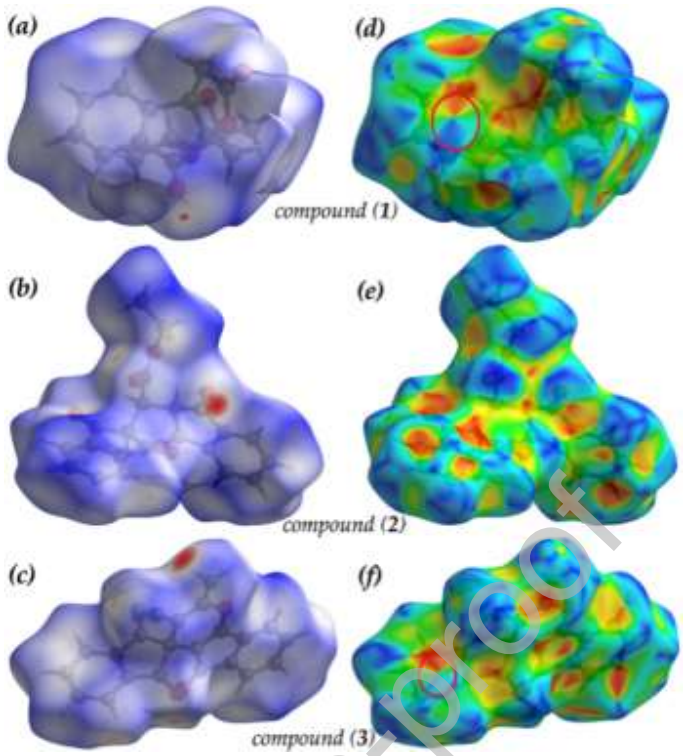

Fig. 5 Hirshfeld surfaces mapped with d_{norm} (left column) (*a–c*) and shape-index (right column) (*d–f*) of the title compounds (**2**–**4**).

The adjacent red and blue triangles (highlighted by red circles) on the shape-index figures (Fig. 5) of compound (**2**) and (**4**) indicates that the molecules are related to one another by π–π stacking interactions [57-59]. The red and blue triangles on the shape index figures characterized the face-to-face π-stacking interaction and in agreement with the geometrical parameters obtained from X-ray structural studies. The scattered points in the breakdown fingerprint plot show that the π–π stacking interactions comprises 3.2%, 1.4% and 4.7% in (**2**–**4**) to the total Hirshfeld surface area of the molecules. In (**3**), the breakdown fingerprint plot shows that π–π stacking comprises only 1.4% but there is no signature on the shape-index surface. Therefore, it can be concluded that the contributions comes from C···C close-contacts only. The scattered points that are displayed as blue/green colour on the diagonals of the fingerprint plots (Figs. S6–S8) at around d_i=d_e= 1.697Å, d_i=d_e= 1.818Å and d_i=d_e= 1.692Å in (**2**–**4**) respectively. The d_{norm} surfaces are also decomposed corresponding to various interactions involved within the structures of (**2**–**4**) that are included in Figs. S9–S11. Another significant contribution comes from H···H contacts that contributed 52.9%, 39.6% and 21.3% to the total Hirshfeld surface area of in (**2**–**4**) respectively. The difference between the molecular interactions due to H···H contacts

are reflected in the distribution of scattered points of the fingerprint plots (Figs. S6–S8), which spread only up to d_i=d_e= 1.136Å, d_i=d_e= 1.086Å and d_i=d_e= 1.232Å in (**2–4**) respectively.

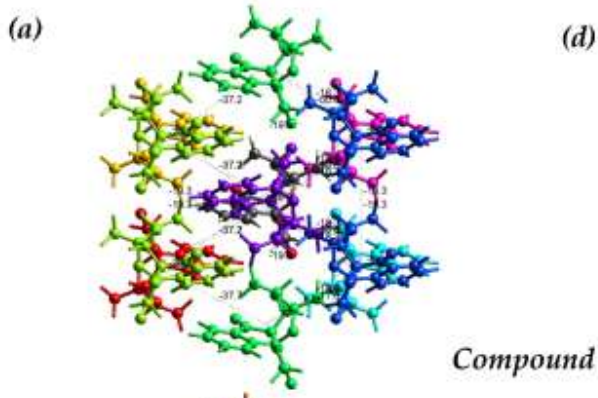

(d)

	N	Symop	R	E_ele	E_pol	E_dis	E_rep	E_tot
	1	-x, -y, -z	6.87	-9.4	-2.9	-37.7	13.0	-36.9
	1	-x, -y, -z	6.76	-9.5	-4.5	-37.7	19.2	-34.3
	2	-x, y+1/2, -z+1/2	10.39	0.7	-0.7	-9.6	5.4	-4.8
	2	x, y, z	7.55	-3.8	-2.6	-22.9	13.1	-17.8
	1	-x, -y, -z	8.11	-24.0	-9.0	-25.6	17.8	-43.3
	2	-x, y+1/2, -z+1/2	7.79	-3.6	-1.2	-25.0	14.1	-17.8
	2	x, -y+1/2, z+1/2	8.18	-11.3	-3.8	-14.8	7.9	-22.8
	1	-x, -y, -z	8.01	-5.2	-2.0	-21.7	13.7	-17.4

Compound (2)

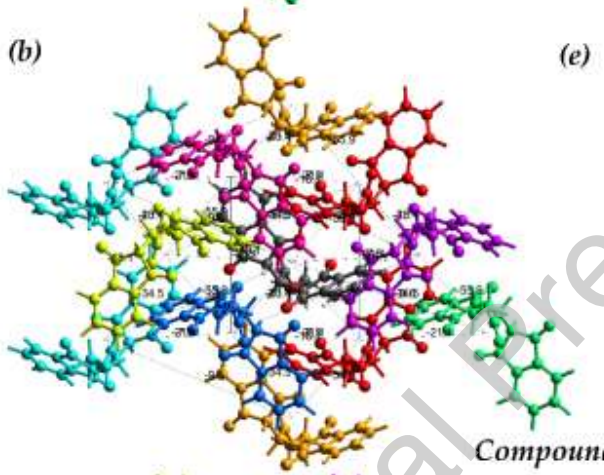

(e)

	N	Symop	R	E_ele	E_pol	E_dis	E_rep	E_tot
	2	-x+1/2, y+1/2, -z+1/2	6.18	-19.5	-8.1	-56.7	35.5	-54.1
	1	x, y, z	9.02	-8.0	-1.7	-15.1	9.2	-17.1
	1	x+1/2, -y+1/2, z+1/2	9.58	-0.6	-0.5	-13.3	8.0	-7.6
	0	-x, -y, -z	10.14	-5.4	-1.8	-22.8	11.2	-20.0
	0	-x, -y, -z	13.52	-1.3	-0.5	-11.7	7.6	-7.2
	0	-x+1/2, y+1/2, -z+1/2	11.82	-3.1	-1.3	-5.3	1.3	-8.0
	0	-x, -y, -z	7.16	-22.2	-5.7	-24.7	22.9	-35.2
	1	-x, -y, -z	10.53	3.1	-0.4	-7.4	1.2	-2.7
	2	x+1/2, -y+1/2, z+1/2	10.42	-9.1	-3.0	-26.3	23.1	-20.5
	1	-x, -y, -z	7.70	-3.3	-1.5	-46.6	17.0	-34.7

Compound (3)

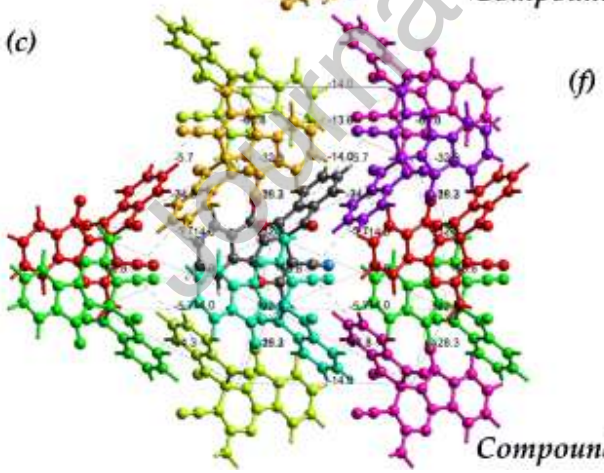

(f)

	N	Symop	R	E_ele	E_pol	E_dis	E_rep	E_tot
	2	x, y, z	10.27	-3.0	-1.5	-15.4	5.5	-14.3
	1	-x, -y, -z	7.48	-7.3	-5.1	-36.3	25.9	-27.1
	2	-x, y+1/2, -z+1/2	8.75	-23.4	-6.7	-23.1	27.4	-32.9
	2	x, -y+1/2, z+1/2	13.03	-8.6	-3.0	-5.9	8.3	-11.3
	2	x, -y+1/2, z+1/2	6.27	-27.9	-12.3	-53.8	36.5	-62.9
	1	-x, -y, -z	6.24	2.6	-4.5	-47.3	34.9	-20.2
	1	-x, -y, -z	10.95	-17.5	-5.1	-30.4	24.4	-33.7
	1	-x, -y, -z	9.32	-14.5	-3.9	-11.9	12.7	-20.7
	2	-x, y+1/2, -z+1/2	11.51	-0.2	-1.1	-7.4	2.4	-5.9

Compound (4)

Fig. 6 The colour-coded interaction mapping for the clusters within 3.8 Å of the compounds (**2-4**) (*a–c*) and the parameters for lattice energy calculations are illustrated in (*d–f*) for compounds (**2-4**) respectively (CHANGE COMPOUND CODES IN THE FIGURE).

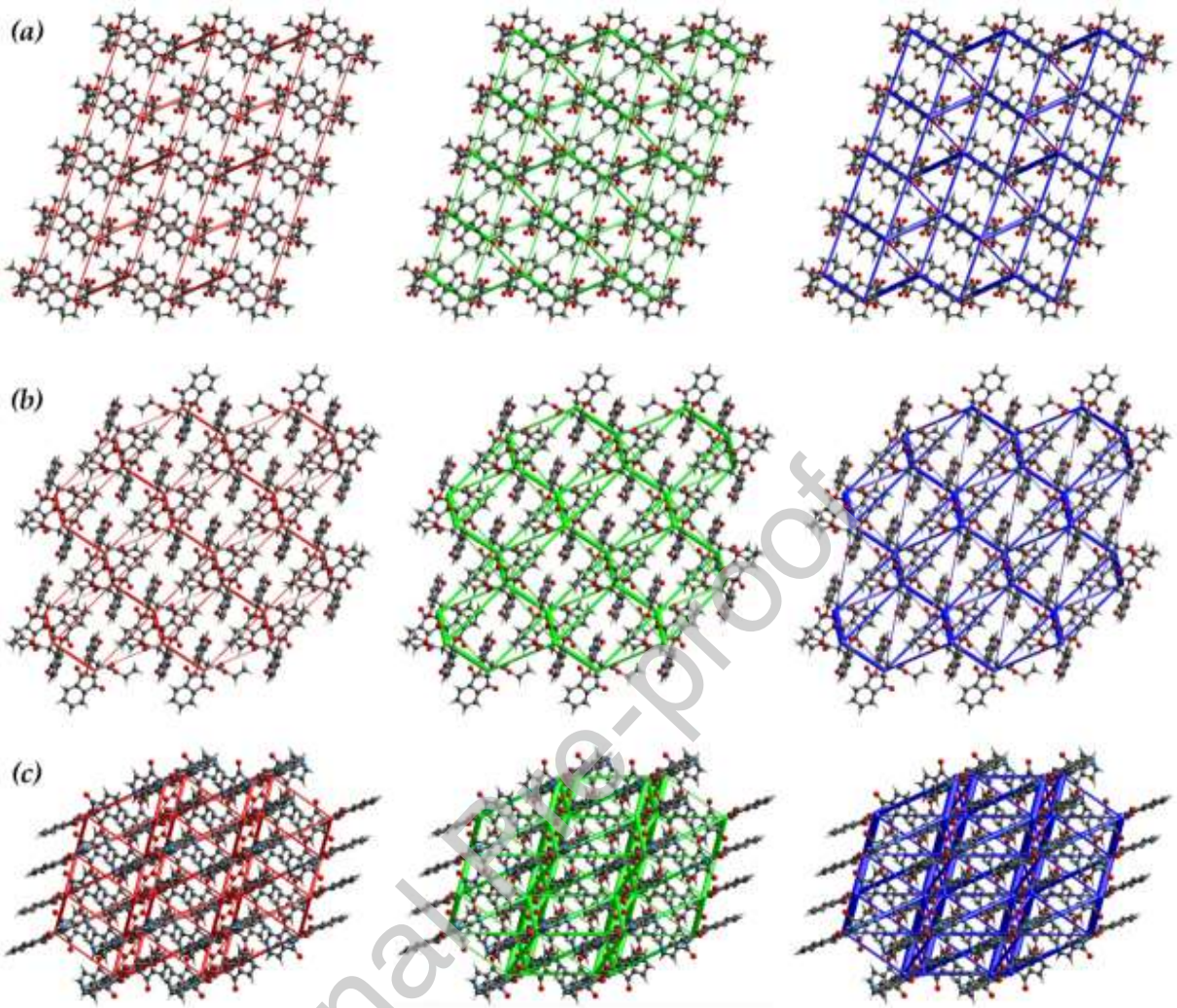

Fig. 7 Energy framework of compounds (**2**–**4**) (*a*-*c*) as viewed down *b*-axis showing the electrostatic potential force (left column), dispersion force (middle column) and total energy (right column) diagrams. The cylindrical radii are proportional to the relative strength of the corresponding energies and they were adjusted to the same scale factor of 80 with a cut-off value of 5 kJ/mol within 2 × 2 × 2 unit cells.

For better understanding of the molecular contacts that are involved within the structures, we have calculated the interaction energies by mapping the structure-cluster within 3.8 Å in a colour-coded molecular cluster related to the specific interaction energy (Fig. 6*a*-*c*). The interaction energies of the available contacts i.e., the energy components (E_{ele}, E_{pol}, E_{dis} and E_{rep}) in addition to the sum of energy components (E_{tot}) for the interactions relative to the reference molecule (based on the colour scheme) for compounds (**2**–**4**) are included in Fig. 6 (*d*-*f*). Moreover, other parameters for lattice energy calculations such as rotational symmetry

operations with respect to the reference molecule (Symop), intercentroid distance between the reference molecule and interacting molecules (R), number of pair(s) of interacting molecules with respect to the reference molecule (N) have been included in Fig. 6(d-f). We have performed the energy frameworks to investigate the overall topology of the energy distribution of (**2**–**4**) by using the scale factor 80 with a cut-off energy value of 5 kJ/mol (Fig. 7). In all compounds, the dispersion force dominates the electrostatic potential force. The dispersion forces in compounds (**2**) and (**3**) dominate the calculation shows that the electrostatic force attributed to the weak H-bonds. In compound (**4**), the electrostatic force attributed to the strong N–H···O interactions and are also dominated by the dispersion forces. The dispersion force co-exists with the main energy framework due to π–π interactions that facilitated to endure the molecular packing of the title compounds. The energy frameworks (Fig. 7) indicates their overall participation in distinct modes of supramolecular association.

3.5. Theoretical calculations

To analyze the non-covalent interactions described above for compounds (**2**–**4**), we have performed theoretical DFT study focusing on the energetic features of the interactions. For the calculations, the crystallographic coordinates have been used and the fragments are modified to evaluate the contributions of different interactions. Following the self-assembled structure (Fig. 2b) of compound (**2**), we have shown two simplified models (see the red arrow in Fig. S12). The first theoretical model is simplified to avoid intramolecular C–H···π interaction and to evaluate the formation energy only. In first model, the binding energy corresponding to weak π–π stacking interaction is ΔE_1 = -0.2 kcal/mol (Fig. S12).

For compound (**3**), we have prepared three simplified models (see red arrows in Fig. 8) to evaluated weak hydrogen bonds and lone-pair(l.p)···π interaction. In the second model (Fig. 8a) the interaction energy for C(15)–H(15)···O(4) bond is ΔE_2 = -1.3 kcal/mol. In another model, we have estimated the formation energy of the centrosymmetric dimer generated through the hydrogen bond C(8)–H(8)···O(3). The interaction energy of the dimeric unit is ΔE_3 = -3.6 kcal/mol (Fig. 8b). Therefore, the formation energy corresponding to one C(8)–H(8)···O(3) hydrogen bond is $\Delta E_3'$ = -3.6/2 = -1.8 kcal/mol which is more favourable than C(15)–H(15)···O(4) hydrogen bond (ΔE_2 = -1.3 kcal/mol). The formation energy corresponding to lone-pair(l.p)···π interaction is ΔE_4 = -1.0 kcal/mol (Fig. 8c).

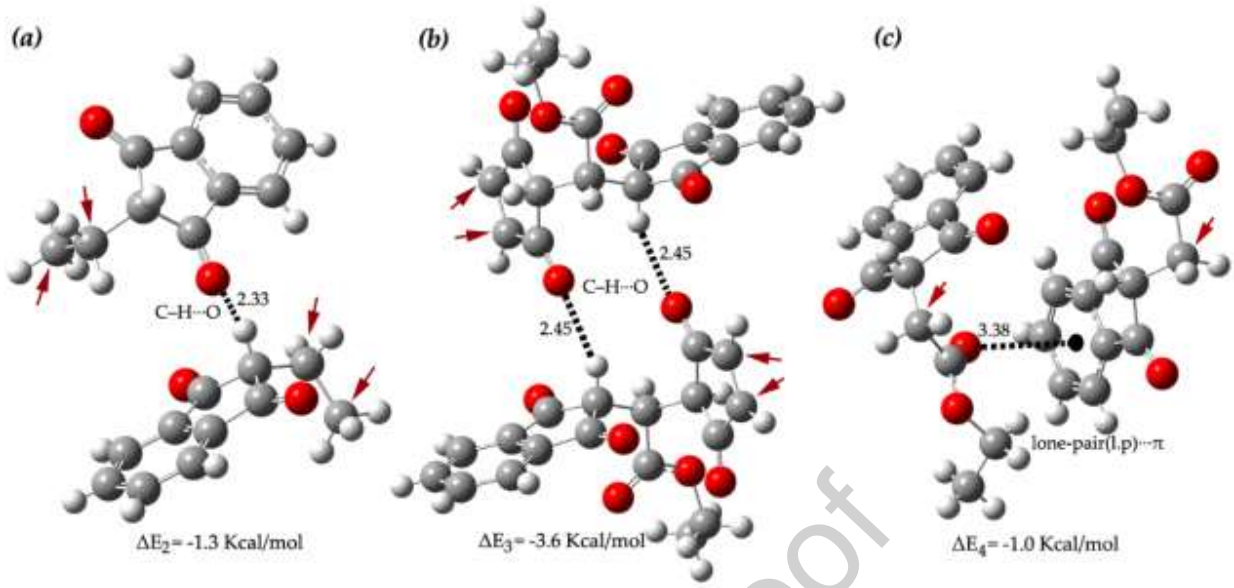

Fig. 8 Theoretical models of compound (**3**) and their interaction energies. Distances in Å.

In Fig. 9, we show the theoretical models to estimate the binding energies in compound (**4**). The binding energy of the C–H···O bonded centrosymmetric dimer is ΔE_5 = -4.5 kcal/mol and is more favorable than the dimer formed in compound (**3**) (ΔE_3 = -3.6 kcal/mol). We also calculated the formation energies for N–H···O hydrogen bonds where an amine nitrogen atom is in contact with two carbonyl oxygen atoms and the models are included in Figs. 9b and 9c respectively. The interaction energy corresponding to the models are -4.1 kcal/mol and -2.9 kcal/mol. Therefore, the N–H···O hydrogen bond of the theoretical model (Fig. 9b) is much more favorable compare to the model included in Fig. 9c.

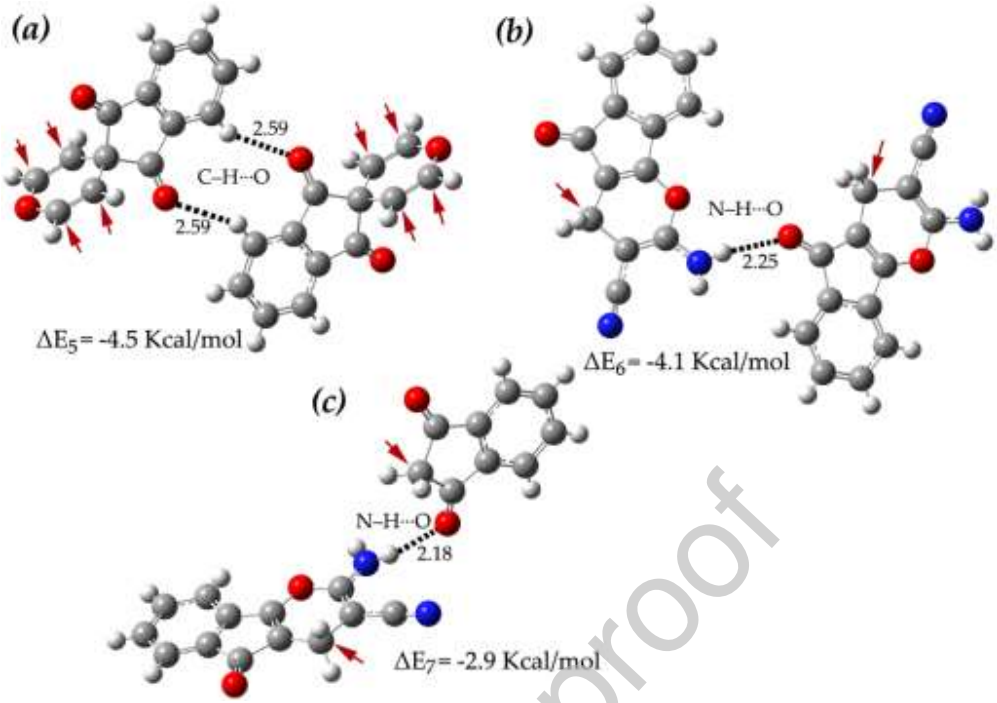

Fig. 9 Theoretical models of compound (**4**) and their interaction energies. Distances in Å.

We have further analyzed the self-assembled dimers of compounds (**2**–**4**) using Bader's theory of "atoms in molecules" (AIM), to provide additional insight on the non-covalent interactions. The AIM analysis provides an unambiguous definition of chemical bonding and therefore used to visualize and characterize non-covalent interactions following the distribution of bond paths and bond critical points (CPs) [52]. Following the X-ray structure described above, the C–H···π interaction is characterized by the CP (ρ_{BCP} = 0.0037 a.u.) and the bond path connecting the methyl hydrogen and carbon atom of the aryl ring (Fig. 10a). Again in Fig. 10a, the CP(ρ_{BCP} = 0.0030 a.u.) and the bond path connecting the carbon atoms of the aryl rings of parent and partner molecule characterizes π–π stacking interaction in (**2**). In compound (**3**), the lone-pair···π interaction is characterized by the bond path connecting carbonyl oxygen and aryl ring carbon atoms (Fig. 10b) and the CP (ρ_{BCP} = 0.0025 a.u.). Finally, the face-to-face π–π stacking in (**4**) is characterized by the CP (ρ_{BCP} = 0.0067 a.u.) and bond path connecting two carbon atoms of the aryl rings of parent and partner molecules (Fig. 10c).

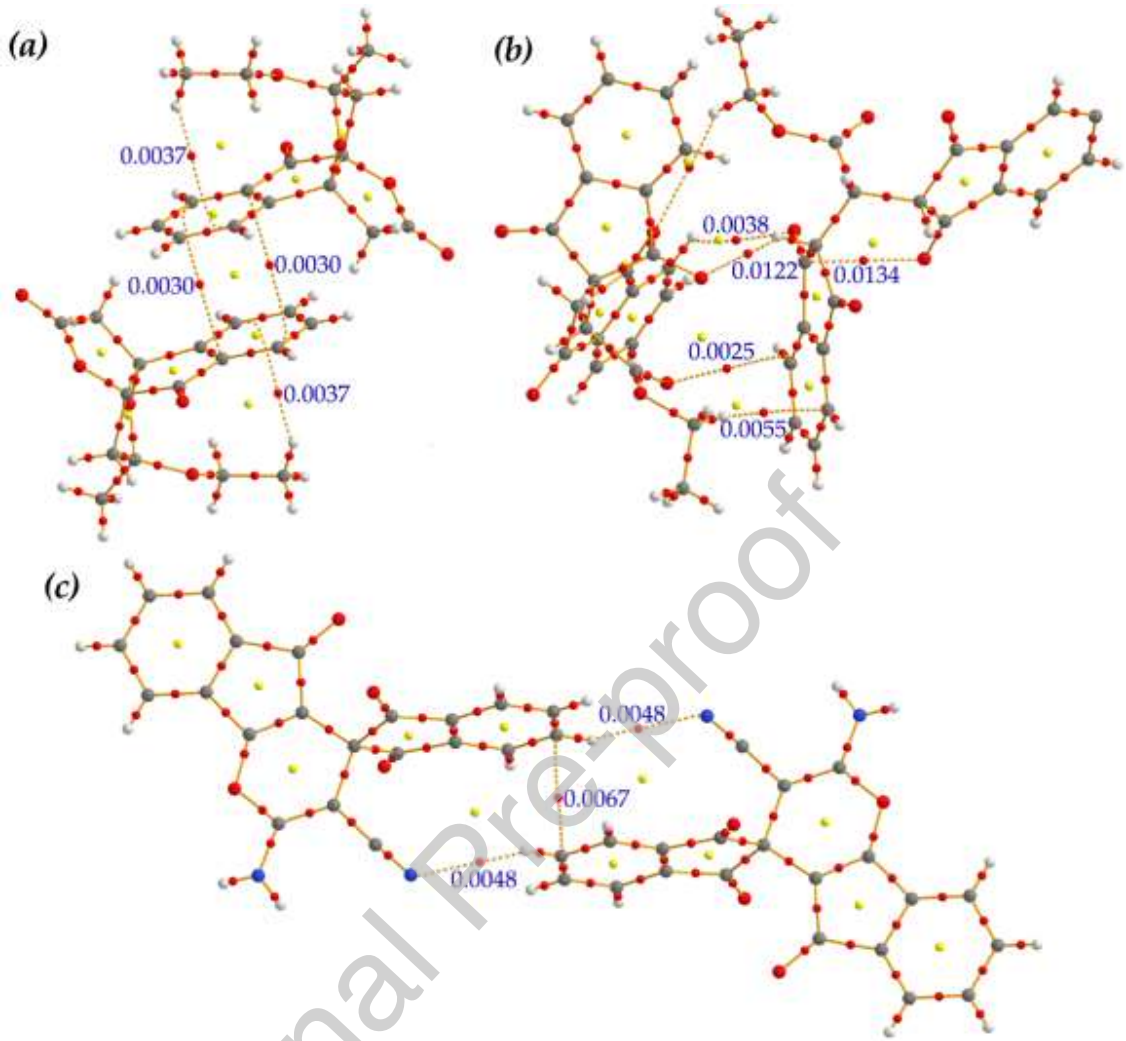

Fig. 10 AIM analysis of the self-assembled dimers retrieved from the X-ray structure of compound (**2**) (*a*), compound (**3**) (*b*) and compound (**4**) (*c*). Red and yellow spheres represent the bond and ring critical points, respectively. The bond path connecting the bond critical points are represented by dashed lines. The values of the ρ(r) at the bond critical points are given in atomic units (a.u.).

4. Conclusions

In summary, three new ninhydrin derivatives have been synthesized and structurally characterized by single-crystal X-ray diffraction. They participate in unprecedented cooperative C–H···π, π–π and lp···π interactions that generates extended supramolecular frameworks. A comparison of the Hirshfeld surfaces of the title compounds have been presented which reveals that more than two-third of the close contacts are associated with weak noncovalent interactions. The interaction energy calculations showed that the contacts between the molecules are largely

dispersive in nature and that are verified by the energy framework of the molecules. The intermolecular interactions have been evaluated using theoretical calculations and AIM analyses that confirm the existence of the interactions. Furthermore, the computational study estimated the contribution of noncovalent interaction to the self-assembly process by providing individual energy values to them. These π-facial interactions in ninhydrin derivatives might have potential importance in the field of drug design and supramolecular chemistry.

Conflicts of interest

There are no conflicts to declare.

Acknowledgements

S. K. Seth gratefully acknowledges the financial support from SERB (NewDelhi) India, for Research Project (EEQ/2019/000384). The financial support from the RUSA 2.0 programme of Jadavpur University is also acknowledged.

Supplementary information

CCDC 1900911, 1900913 and 1900912 contain the supplementary crystallographic data of compounds (**2**–**4**) respectively. These data can be obtained free of charge via http://www.ccdc.cam.ac.uk/conts/retrieving.html, or from the Cambridge Crystallographic Data Centre,12 Union Road, Cambridge CB21EZ, UK; fax: (+44) 1223-336-033; or E-mail:deposit@ccdc.cam.ac.uk. The full and breakdown fingerprint plots are included as supplementary data.

Credit Author Statement

Kamal K. Kapoor gave the planning of the synthesis of the compounds, Yeshwinder Saini and Sheena Mahajan synthesized the compounds and other physico-chemical experiments. Geeta Hundal solved the structures. Saikat Kumar Seth, Yeshwinder Saini and Kamal K. Kapoor analyzed the data. Saikat Kumar Seth contributed performing the theoretical calculations; Saikat Kumar Seth and Yeshwinder Saini wrote the paper.

Declaration of Interest Statement.

The authors declare no competing financial interest.

References

[1] (a) L. H. Zalkov, R. N. I. Harris,D. V. Derveer, Modhephene: a sesquiterpenoid carbocyclic[3.3.3]propellane. *X*-Ray crystal structure of the corresponding diol, J. Chem. Soc., Chem. Commun. (1978) 420–421;

(b) F. Bohlmann, C. Zdero,R. Bohlmann, R. M. King, H. Robinson, Neue sesquiterpene aus *Liabum*-arten, Phytochemistry, 19 (1980) 579–582.

[2] (a) Y. Sugimoto, H. A. A. Babiker, T. Saisho, T. Furumoto, S. Inanaga,M. Kato, Chlorinated Alkaloids in *Menispermum dauricum* DC. Root Culture, J. Org. Chem. 66 (2001) 3299–3302;

(b) M. Tomita, Y. Okamoto, T. Kikuchi, K. Osaki, M. Nishikawa, K. Kamiya, Y. Sasaki, K. Matoba, K. Goto, Acutumine and acutumidine, chlorine containing alkaloids with a novel skeleton (1): X-ray analysis of acutumine, Tetrahedron Lett.8 (1967) 2421–2424;

(c) M. Nishikawa, K. Kamiya, M. Tomita, Y. Okamoto, T. Kikuchi, K. Osaki, Y. Tomiie, I. Nitta, K. Goto,The *X*-ray analyses of acutumine and its acetate; a trial of a short cut in the structure elucidation, J. Chem. Soc. B6 (1968) 652–658;

(d) B. W. Yu, J. Y. Chen, Y. P. Wang, K. F Cheng, X. Y. Li, G. W. Qin, Alkaloids from *Menispermum dauricum*, Phytochemistry 61 (2002) 439–442;

(e) G. W. Qin, X.C. Tang, D.H. Caignard, P. Renard, P. Lestage, *Patent No. WO2004000815*, 2003.

[3] H. Jian-Mei, Y. Ritsuko, Y. Chun-shu, Y. Fukuyama, Merrilactone A, a novel neurotrophic sesquiterpene dilactone from *Illicium merrillianum*, Tetrahedron Lett. 41 (2000) 6111–6114.

[4] T. Ibuka, K. Tanaka, Y. Inubushi, Total Synthesis of the Alkaloid, (±)-Hasubanonine, Chem. Pharm. Bull. 22 (1974) 782–798.

[5] U. Bach, K. De Cloedt, H.Spretizer, M. Gratzel,Characterization of Hole Transport in a New Class of Spiro-Linked Oligotriphenylamine Compounds, Adv. Mater. 12 (2000) 1060–1063.

[6] (a) S. Udenfriend, S. Stein, P. Böhlen, W. Dairman, W. Leimgruber, M. Weigele, Fluorescamine: A Reagent for Assay of Amino Acids, Peptides, Proteins, and Primary Amines in the Picomole Range, Science178 (1972) 871;

(b) K. Debnath, S. Pathak, A. Pramanik,Silica Sulfuric Acid: An Efficient Reusable Heterogeneous Solid Support for the Synthesis of 3H,3′H-Spiro[benzofuran-2,1′isobenzofuran]-3,3′-diones under Solvent-Free Condition, Tetrahedron Lett. 55 (2014) 1743–1748.

[7] M. Gerlitz, H. Olivan, M. Kurz, PCT Int. Appl. WO 2010012381 A1.

[8] Y. Malpani, R. Achary, S. Y. Kim, H. C. Jeong, P. Kim, S. B. Han, M. Kim, C. -K. Lee, J. N. Kim, Y. -S. Jung, Efficient synthesis of 3*H*,3′*H*-spiro[benzofuran-2,1′-isobenzofuran]-3,3′-dione as novel skeletons specifically for influenza virus type B inhibition, Eur. J. Med. Chem. 62 (2013) 534–544.

[9] J. Finn, X. Y. Yu, Z. G. Wang, J. Hill, D. Keith, P. Gallant, P. Wendler, PCT Int. Appl. WO 0018772, 2000; Chem. Abstr. 132 (2000) 251137.

[10] (a) E. J. Corey, X. –M. Cheng, *The Logic of Chemical Synthesis*, Wiley: NY, 1989;

(b) M. D. Levin, P. Kaszynski, J. Michl, Bicyclo[1.1.1]pentanes, [*n*]Staffanes, [1.1.1] Propellanes, and Tricyclo[2.1.0.0^{2,5}]pentanes, Chem. Rev. 100 (2000) 169–234;

(c) Y. Ito, V. Y. Lee, H. Gornitzka, C. Goedecke, G. Frenking, A. Sekiguchi,Spirobis(pentagerma [1.1.1]propellane): A Stable Tetraradicaloid, J. Am. Chem. Soc. 135 (2013) 6770–7773.

[11] Y. Saini, R. Khajuria, L. K. Rana, M. S. Hundal, V. K. Gupta, R. Kant and K. K. Kapoor, Unprecedented reaction of ninhydrin with ethyl cyanoacetate and diethyl malonate on ultrasonic irradiation, Tetrahedron 72 (2016) 257–263.

[12] G. R. Desiraju, *The Design of Organic Solids, Materials Science Monographs 54*, Elsevier, Amsterdam, 1989.

[13] B. Moulton, M. J. Zaworotko, From Molecules to Crystal Engineering: Supramolecular Isomerism and Polymorphism in Network Solids, Chem. Rev. 101 (2001) 1629–1658.

[14] J. W. Steed, J. L. Atwood, *Supramolecular Chemistry*,Wiley, Chichester, 2nd edn, 2009.

[15] Comprehensive Supramolecular Chemistry II, ed. J. L. Atwood, G. W. Gokel, L. J. Barbour, Elsevier, 2017.

[16] K. Biradha,Crystal engineering: from weak hydrogen bonds to co-ordination bonds, CrystEngComm 5 (2003) 374–384.

[17] M. R. Shimpi, S. P. Velaga, F. U. Shah, O. N. Antzutkin, Pharmaceutical Crystal Engineering Using Ionic Liquid Anion–Solute Interactions, Cryst. Growth Des.17 (2017) 1729–1734.

[18] G. R. Desiraju, Crystal Engineering: A Holistic View, Angew. Chem., Int. Ed. 46 (2007) 8342–8356.

[19] P. Seth, A. Bauzá, A. Frontera, C. Massera, P. Gamez, A.Ghosh, Analysis of the contribution of the π-acidity of the *s*-tetrazine ring in the crystal packing of coordination polymers, Cryst. Eng. Comm.15 (2013) 3031–3039.

[20] T. Maity, H. Mandal, A. Bauza, B. C. Samanta, A. Frontera, S. K. Seth, Quantifying conventional C–H···π(aryl) and unconventional C–H···π(chelate) interactions in dinuclear Cu(II) complexes: experimental observations, Hirshfeld surface and theoretical DFT study, New J. Chem. 42 (2018) 10202–10213.

[21] S. K. Seth, D. Sarkar, T. Kar, Use of π–π forces to steer the assembly of chromone derivatives into hydrogen bonded supramolecular layers: crystal structures and Hirshfeld surface analyses, Cryst. Eng. Comm.13 (2011) 4528–4535.

[22] S. K. Seth, D. Sarkar, A. D. Jana, T. Kar, On the Possibility of Tuning Molecular Edges To Direct Supramolecular Self-Assembly in Coumarin Derivatives through Cooperative Weak Forces: Crystallographic and Hirshfeld Surface Analyses, Cryst. Growth Des.11 (2011) 4837–4849.

[23] S. K. Seth, P. Manna, N.J. Singh, M. Mitra, A.D. Jana, A. Das,S.R. Choudhury, T. Kar, S. Mukhopadhyaya, K.S. Kim,Molecular architecture using novel types of non-covalent π-

interactions involving aromatic neutrals, aromatic cations and π-anions, CrystEngComm 15 (2013) 1285–1288.

[24] P. Manna, S. K. Seth, M. Mitra, A. Das, N. J. Singh, S.R.Choudhury, T. Kar, S. Mukhopadhyay,A successive layer-by-layer assembly of supramolecular frameworks driven by a novel type of face-to-face π^+–π^+ interactions, Cryst.Eng.Comm.15 (2013) 7879–7886.

[25] A. Frontera, P. Gamez, M. Mascal, T.J. Mooibroek, J.Reedijk,Putting Anion–π Interactions Into Perspective, Angew. Chem. Int. Ed. 50 (2011) 9564–9583.

[26] P. Manna, S.K. Seth, M. Mitra, S.R. Choudhury, A. Bauzá, A.Frontera, S. Mukhopadhyay, Experimental and Computational Study of Counterintuitive ClO_4^- ⋯ClO_4^- Interactions and the Interplay between π^+–π and Anion⋯π^+ Interactions, Cryst. Growth Des. 14 (2014) 5812–5821.

[27] P. Manna, S.K. Seth, A. Bauzá, M. Mitra, S.R. Choudhury, A. Frontera, S. Mukhopadhyay,Dependent Formation of Unprecedented Water–Bromide Cluster in the Bromide Salts of PTP Assisted by Anion−π Interactions: Synthesis, Structure, and DFT Study, Cryst. Growth Des. 14 (2014)747–755.

[28] M. Mitra, P. Manna, A. Bauzá, P. Ballester, S.K. Seth, S.R. Choudhury, A. Frontera, S. Mukhopadhyay,3-Picoline Mediated Self-Assembly of M(II)–Malonate Complexes (M = Ni/Co/Mn/Mg/Zn/Cu) Assisted by Various Weak Forces Involving Lone Pair−π, π–π, and Anion⋯π–Hole Interactions, J. Phys.Chem. B. 118 (2014) 14713–14726.

[29] B. Notash, N. Safari, H.R. Khavasi,Anion-controlled structural motif in one-dimensional coordination networks *via* cooperative weak non covalent interactions, Cryst. Eng. Comm.14 (2012) 6788–6796.

[30] S.K. Seth, I. Saha, C. Estarellas, A. Frontera, T. Kar, S.Mukhopadhyay, Supramolecular Self-Assembly of M-IDA Complexes Involving Lone-Pair⋯π Interactions: Crystal Structures, Hirshfeld Surface Analysis, and DFT Calculations [H_2IDA = iminodiacetic acid, M = Cu(II), Ni(II)], Cryst. Growth Des. 11 (2011) 3250–3265.

[31] P. Manna, S.K. Seth, A. Das, J. Hemming, R. Prendergast, M.Helliwell, S.R. Choudhury, A. Frontera, S. Mukhopadhyay, Anion Induced Formation of Supramolecular

Associations Involving Lone pair−π and Anion−π Interactions in Co(II) Malonate Complexes: Experimental Observations, Hirshfeld Surface Analyses and DFT Studies, Inorg. Chem. 51 (2012) 3557–3571.

[32] I. Alkorta, F. Blanco, P.M. Deya, J. Elguero, C. Estarellas, A. Frontera, D. Quinonero,Cooperativity in multiple unusual weak bonds, Theor. Chem. Acc. 126 (2010) 1–14.

[33] J.W. Steed, D.R. Turner, K.J. Wallace, Core Concepts inSupramolecular Chemistry and Nanochemistry; John Wiley &Sons, Ltd.: Chichester, UK, 2007; pp. 194–228.

[34] B. S. Furniss, A. J. Hannaford, P. W. G. Smith, *Vogel's Textbook of Practical Organic Chemistry 5th ed. Addition WesleyLongman Limited- England*, 1989.

[35] Bruker, *SAINT, Version 6.36a*, Bruker AXS Inc., Madison, Wisconsin, USA, 2002.

[36] Bruker, *SMART, Version 5.625* and *SADABS, Version 2.03a*,Bruker AXS Inc., Madison, Wisconsin, USA, 2001.

[37] G. M. Sheldrick, A short history of *SHELX*, ActaCrystallogr., Sect. A 64 (2008) 112–122.

[38] G. M. Sheldrick,Crystal structure refinement with *SHELXL*, ActaCrystallogr., Sect. C, 71 (2015) 3–8.

[39] M.A. Spackman, J.J. McKinnon,Fingerprinting intermolecular interactions in molecular crystals, CrystEngComm 4 (2002)378–392.

[40] J. J. McKinnon, D. Jayatilaka, M. A. Spackman,Towards quantitative analysis of intermolecular interactions with Hirshfeld surfaces, Chem. Commun. (2007) 3814–3816.

[41] F. P. A. Fabbiani, L. T. Byrne, J. J. McKinnon, M. A.Spackman,Solvent inclusion in the structural voids of form II carbamazepine: single-crystal X-ray diffraction, NMR spectroscopy and Hirshfeld surface analysis, CrystEngComm 9 (2007) 728–731.

[42] S. K. Seth, Tuning the formation of MOFs by pH influence: X-ray structural variations and Hirshfeld surface analyses of 2-amino-5-nitropyridine with cadmium chloride, CrystEngComm 15 (2013) 1772–1781.

[43] M. A. Spackman, P. G. Byrom, A novel definition of a molecule in a crystal, Chem. Phys. Lett. 267 (1997) 215–220.

[44] J. J. McKinnon, A. S. Mitchell, M. A. Spackman,Hirshfeld Surfaces: A New Tool for Visualising and Exploring Molecular Crystals, Chem. Eur. J. 4 (1998) 2136–2141.

[45] J. J. McKinnon, M. A. Spackman, A. S. Mitchell, Novel Tools for Visualizing and Exploring Intermolecular Interactions in Molecular Crystals, Acta Crystallogr. B. 60 (2004) 627–668.

[46] A. L. Rohl, M. Moret, W. Kaminsky, K. Claborn, J. J. Mckinnon,B. Kahr, Hirshfeld Surfaces Identify Inadequacies in Computations of Intermolecular Interactions in Crystals: Pentamorphic 1,8-Dihydroxyanthraquinone, Cryst. Growth Des. 8 (2008) 4517–4525.

[47] (a) S. K. Seth, Structural characterization and Hirshfeld surface analysis of a Co^{II} complex with imidazo[1,2-a]pyridine, Acta Cryst. E74 (2018) 600–606;

(b) S. K. Seth, The Importance of CH···X (X = O, π) Interaction of a New Mixed Ligand Cu(II) Coordination Polymer: Structure, Hirshfeld Surface and Theoretical Studies, Crystals 8 (2018) 455.

[48] M. J. Turner, J. J. McKinnon, S. K. Wolff, D. J. Grimwood, P. R. Spackman, D. Jayatilaka, M. A. Spackman, *CrystalExplorer17*; University of Western Australia, 2017.

[49] C. F. Mackenzie, P. R. Spackman, D. Jayatilaka, M. A. Spackman, IUCrJ, *Crystal Explorer* Model Energies and Energy Frameworks: Extension to Metal Coordination Compounds, Organic Salts, Solvates and Open-Shell Systems 4 (2017) 575–587.

[50] M. J. Turner, S. P. Thomas, M. W. Shi, D. Jayatilaka, M. A. Spackman,Energy frameworks: insights into interaction anisotropy and the mechanical properties of molecular crystals, Chem. Commun. 51 (2015) 3735–3738.

[51] M. J. Frisch, G. W. Trucks, H. B. Schlegel, G. E. Scuseria, M. A. Robb, J. R. Cheeseman, G. Scalmani, V. Barone, G. A. Petersson, H. Nakatsuji, X. Li, M. Caricato, A. V. Marenich, J.Bloino, B. G. Janesko, R. Gomperts, B. Mennucci, H. P.Hratchian, J. V. Ortiz, A. F. Izmaylov, J. L. Sonnenberg, D.Williams-Young, F. Ding, F. Lipparini, F. Egidi, J. Goings, B. Peng, A. Petrone, T. Henderson, D. Ranasinghe, V. G.Zakrzewski, J. Gao, N. Rega, G. Zheng, W. Liang, M. Hada,M. Ehara, K. Toyota, R. Fukuda, J. Hasegawa, M. Ishida, T. Nakajima, Y. Honda, O. Kitao, H. Nakai, T. Vreven, K. Throssell, J. A. Montgomery Jr., J. E. Peralta, F. Ogliaro, M. J.Bearpark, J. J. Heyd, E. N. Brothers, K. N. Kudin, V. N. Staroverov, T. A. Keith, R. Kobayashi, J. Normand, K. Raghavachari, A. P. Rendell, J. C. Burant, S. S. Iyengar, J. Tomasi, M. Cossi, J. M. Millam, M. Klene, C. Adamo, R. Cammi, J. W. Ochterski, R. L. Martin, K. Morokuma, O. Farkas, J. B. Foresman, D. J. Fox, Gaussian 09, Revision C.01, Gaussian, Inc., Wallingford, CT, 2009.

[52] R.F.W. Bader, A quantum theory of molecular structure and its applications, Chem. Rev. 91 (1991) 893–928.

[53] T.A. Keith, *AIMAll* (version 13.05.06), TK Gristmill Software, Overland Park, KS, USA, 2013.

[54] R.F.W. Bader, Atoms in Molecules, A Quantum Theory, Oxford University Press, New York, 1990.

[55] (a) A. Schonberg, E. Singer, NON-CATALYTIC ALDOL ADDITIONS WITH HYDRATE-FORMING KETO CARBONYL COMPOUNDS, Chem. Ber. 103 (1970) 3871;

(b) M. R. Bryce, S. R. Davies, M. Hasan, G. J. Ashwell, M.Szablewski, M. G. B. Drew, R. Short, M. B. Hursthouse, Preparation and magnetic properties of a range of metal and organic cation salts of 2,3-dicyano-\1,4-naphthoquinone (DCNQ). *X*-Ray crystal structure of (methyltriphenylphosphonium)$_1$(DCNQ)$_1$ (H_2O)$_1$ and 2-dicyanomethylene-indan-1,3-dione (DCID). The rearrangement of DCID to DCNQ, J. Chem. Soc. Perkin Trans 2 (1989) 1285-1292;

(c) S. Chatterjee, Studies of the charge-transfer complexes of 2-dicyanomethyleneindane-1,3-dione, J. Chem. Soc. (B) 1969, 725-729;

(d) M. Chakrabarty, A. Mukherji, S. Arima, Y. Harigaya, G.Pilet, Expeditious reaction of ninhydrin with active methylene compounds on montmorillonite K_{10} clay, Montash Chem.140 (2009) 189–197.

[56] A. Kundu, A. Pramanik, Novel synthesis of a series of spiro 1,3-indanedione-fused-dihydropyridines through the condensation of a tetrone with N-aryl/alkylenamines in presence of solid support silica sulphuric acid, Mol. Divers. 19 (2015) 459–471.

[57] S. K. Seth, N. K. Das, K. Aich, D. Sen, H.-K. Fun, S. Goswami, Exploring contribution of intermolecular interactions in supramolecular layered assembly of naphthyridine co-crystals: Insights from Hirshfeld surface analysis of their crystalline states, J. Mol. Struct. 1048 (2013) 157–165.

[58] S. K. Seth, Structural elucidation and contribution of intermolecular interactions in *O*-hydroxy acyl aromatics: Insights from X-ray and Hirshfeld surface analysis, J. Mol. Struct. 1064 (2014) 70–75.

[59] T. Samanta, L. Dey, J. Dinda, S. K. Chattopadhyay, S.K. Seth, Cooperativity of anion···π and π···π interactions regulates the self-assembly of a series of carbene proligands: Towards quantitative analysis of intermolecular interactions with Hirshfeld surface, J. Mol. Struct. 1068 (2014) 58–70.

GRAPHICAL ABSTRACT